


# Spin-orbit torque effect in silicon-based sputtered $Mn_3Sn$ film

Sha Lu(卢莎), Dequan Meng(孟德全), Adnan Khan, Ziao Wang(王子傲), Shiwei Chen(陈是位), and Shiheng Liang(梁世恒)

**Citation:** Chin. Phys. B, 2024, 33 (**10**): 107501. DOI: 10.1088/1674-1056/ad6079
Journal homepage: http://cpb.iphy.ac.cn; http://iopscience.iop.org/cpb

**What follows is a list of articles you may be interested in**

---

## Dzyaloshinskii-Moriya interaction and field-free sub-10 nm topological magnetism in Fe/bismuth oxychalcogenides heterostructures

Yaoyuan Wang(王垚元), Long You(游龙), Kai Chang(常凯), and Hongxin Yang(杨洪新)
Chin. Phys. B, 2024, 33 (**9**): 097508. DOI: 10.1088/1674-1056/ad6a0e

## Mapping the antiparallel aligned domain rotation by microwave excitation

Jing Zhang(张景), Yuanzhi Cui(崔远志), Xiaoyu Wang(王晓雨), Chuang Wang(王创), Mengchen Liu(刘梦晨), Jie Xu(徐洁), Kai Li(李凯), Yunhe Zhao(赵芸鹤), Zhenyan Lu(陆振烟), Lining Pan(潘丽宁), Chendong Jin(金晨东), Qingfang Liu(刘青芳), Jianbo Wang(王建波), and Derang Cao(曹德让)
Chin. Phys. B, 2024, 33 (**9**): 097506. DOI: 10.1088/1674-1056/ad5536

## RKKY interaction in helical higher-order topological insulators

Sha Jin(金莎), Jian Li(李健), Qing-Xu Li(李清旭), and Jia-Ji Zhu(朱家骥)
Chin. Phys. B, 2024, 33 (**7**): 077503. DOI: 10.1088/1674-1056/ad3ef9

## Oscillation of Dzyaloshinskii-Moriya interaction driven by weak electric fields

Runze Chen(陈润泽), Anni Cao(曹安妮), Xinran Wang(王馨苒), Yang Liu(柳洋), Hongxin Yang(杨洪新), and Weisheng Zhao(赵巍胜)
Chin. Phys. B, 2024, 33 (**2**): 027501. DOI: 10.1088/1674-1056/ad0f85

## Progress on two-dimensional ferrovalley materials

Ping Li(李平), Bang Liu(刘邦), Shuai Chen(陈帅), Wei-Xi Zhang(张蔚曦), and Zhi-Xin Guo(郭志新)
Chin. Phys. B, 2024, 33 (**1**): 017505. DOI: 10.1088/1674-1056/acf65f

---

# Spin–orbit torque effect in silicon-based sputtered $Mn_3Sn$ film

Sha Lu(卢莎)[1,†], Dequan Meng(孟德全)[1,†], Adnan Khan[1], Ziao Wang(王子傲)[1], Shiwei Chen(陈是位)[1,2,‡], and Shiheng Liang(梁世恒)[1,2,§]

[1] *School of Physics, Hubei University, Wuhan* 430062, *China*
[2] *Key Laboratory for Intelligent Sensing System and Security of Ministry of Education, Wuhan* 430062, *China*

(Received 28 April 2024; revised manuscript received 26 June 2024; accepted manuscript online 9 July 2024)

Noncollinear antiferromagnet $Mn_3Sn$ has shown remarkable efficiency in charge–spin conversion, a novel magnetic spin Hall effect, and a stable topological antiferromagnetic state, which has resulted in great interest from researchers in the field of spin–orbit torque. Current research has primarily focused on the spin–orbit torque effect of epitaxially grown noncollinear antiferromagnet $Mn_3Sn$ films. However, this method is not suitable for large-scale industrial preparation. In this study, amorphous $Mn_3Sn$ films and $Mn_3Sn$/Py heterostructures were prepared using magnetron sputtering on silicon substrates. The spin-torque ferromagnetic resonance measurement demonstrated that only the conventional spin–orbit torque effect generated by in-plane polarized spin currents existed in the $Mn_3Sn$/Py heterostructure, with a spin–orbit torque efficiency of 0.016. Additionally, we prepared the perpendicular magnetized $Mn_3Sn$/CoTb heterostructure based on amorphous $Mn_3Sn$ film, where the spin–orbit torque driven perpendicular magnetization switching was achieved with a lower critical switching current density ($3.9\times10^7$ A/cm$^2$) compared to Ta/CoTb heterostructure. This research reveals the spin–orbit torque effect of amorphous $Mn_3Sn$ films and establishes a foundation for further advancement in the practical application of $Mn_3Sn$ materials in spintronic devices.

**Keywords:** spintronics, noncollinear antiferromagnetism, spin–orbit torque

**PACS:** 75.30.Gw, 75.50.Ee, 85.75.–d **DOI:** 10.1088/1674-1056/ad6079

## 1. Introduction

The spin–orbit torque (SOT) effect, based on spin–orbit coupling (SOC), can efficiently manipulate magnetization direction and achieve perpendicular magnetization switching by current injection. This capability is crucial for the development of next-generation ultrafast, high-density, and low-power spintronic, logic, and neuromorphic devices. Consequently, it has attracted extensive attention and research over the past decade.[1–6] Among these efforts, enhancing the efficiency of SOT and achieving deterministic perpendicular magnetization switching without external magnetic fields (i.e., field-free switching) are hot and critical issues in constructing energy-efficient SOT devices.[3–6] Compared with traditional 5d heavy metal materials, the noncollinear antiferromagnetic materials exhibit high spin Hall conductivities, and generate out-of-plane polarized spin currents and corresponding unconventional out-of-plane SOTs due to lower magnetic structure symmetry. These unique characteristics can break the spatial symmetry of perpendicular magnetization and allow for field-free switching. As a result, noncollinear antiferromagnetic materials have become a focal point in SOT research.[7–11]

Hexagonal $Mn_3Sn$ is a typical noncollinear antiferromagnetic material. Below the Néel temperature ($T_N \sim$ 420 K), the Mn atoms exhibit a planar 120° chiral structure within the kagome planes due to geometric frustration and the Dzyaloshinskii–Moriya interaction.[12] This unique noncollinear antiferromagnetic structure gives rise to intriguing properties, including large anomalous Hall effects (AHEs),[13–18] anomalous Nernst effects (ANE),[19–23] antiferromagnetic tunneling magnetoresistance effect,[24] and ultrafast laser-modulated magneto-optical Voigt effect,[25] and topological Weyl fermions[26] induced by topological structures. Recently, related researches have utilized noncollinear antiferromagnetic $Mn_3Sn$ as a spin source to investigate SOT effects. Hu *et al.* successfully achieved efficient current-driven perpendicular magnetization switching without an external magnetic field based on the epitaxial $Mn_3Sn$ films. This field-free switching feature is attributed to the unconventional out-of-plane spin–orbit torque generated by the out-of-plane polarized spin current in $Mn_3Sn$.[8] Bangar *et al.* observed large spin Hall conductivities in epitaxial $Mn_3Sn$ films, attributing them to Fermi level shifts caused by increased Mn atoms in $Mn_3Sn$.[7] Wang *et al.* used magnetic optical Kerr effect and spin-torque ferromagnetic resonance (ST-FMR) methods to observe unconventional spin–orbit torques generated by spin currents with $x$ and $z$ polarizations. These torques were derived from noncollinear spin structures with SOC in $Mn_3Sn$.[27]

While epitaxial $Mn_3Sn$ films demonstrate high spin Hall conductivities and unconventional out-of-plane SOTs, which present great potential for spintronic applications, the epitax-

[†]These authors contributed equally to this work.
[‡]Corresponding author. E-mail: chenshw@hubu.edu.cn
[§]Corresponding author. E-mail: shihengliang@hubu.edu.cn

© 2024 Chinese Physical Society and IOP Publishing Ltd 

ial preparation method based on single crystal substrates is not suitable for large-scale industrial production. Recent studies indicate that amorphous materials exhibit higher SOT efficiencies, spin–orbit Hall conductivities, and lower damping constants compared to epitaxial and polycrystalline films. These discoveries offer new insights into SOT research.[28–31]

In this study, we fabricated the amorphous $Mn_3Sn$ films on Si substrates, $Mn_3Sn$/Py heterostructures and perpendicularly magnetized $Mn_3Sn/Co_{0.64}Tb_{0.36}$ heterostructures by magnetron sputtering system. The experimental results indicated a low damping constant of 0.004 in the $Mn_3Sn$/Py heterostructure. Moreover, we observed a conventional SOT induced by in-plane polarized spin currents, which induces the perpendicular magnetization switching of the ferrimagnetic CoTb with a critical switching current density lower than that of $Ta/Co_{0.64}Tb_{0.36}$ heterostructures. This research provides a new perspective for studying the SOT of $Mn_3Sn$ films and also advances the practical application of $Mn_3Sn$ materials in SOT devices.

## 2. Experiment

Heterostructures of $Mn_3Sn(10)/Si_3N_4(3)$, $Mn_3Sn(10)/Py(7)/Si_3N_4(3)$, and $Mn_3Sn(10)/CoTb(7)/Si_3N_4(3)$, where the numbers in parentheses represent the nominal thicknesses in nanometers, were fabricated on thermally oxidized Si substrates at room temperature by using an ultrahigh-vacuum magnetron sputtering system with a base pressure better than $1.0\times10^{-6}$ Pa. A protective capping layer of $Si_3N_4$ was employed to prevent sample oxidation. The crystalline structure of $Mn_3Sn/Si_3N_4$ film was checked by x-ray diffraction (XRD) and the corresponding results are illustrated in Fig. 1(a). The $\theta$–$2\theta$ pattern revealed the absence of $Mn_3Sn$ diffraction peaks in $Mn_3Sn/Si_3N_4$ films, indicating the amorphous nature of the $Mn_3Sn$ films fabricated by magnetron sputtering. Recently, the AHE has been observed in collinear antiferromagnets[32] and noncollinear antiferromagnets.[13–18] The magneto transport measurement on the silicon-based sputtered $Mn_3Sn$ film is carried out at room temperature, as shown in Fig. 1(b). After subtracting the linear ordinary Hall signal, Fig. 1(b) shows the anomalous Hall resistance ($R_{\rm Hall}$) as a function of the out-of-plane magnetic field of the sputtered $Mn_3Sn$ film, indicating the existing noncollinear spin structure and the resulting nonzero Berry curvature contribution. Figure 1(c) shows the magnetic hysteresis loop of the $Mn_3Sn/Si_3N_4$ films when the external magnetic field is parallel to the film plane. We found that the prepared $Mn_3Sn$ films exhibit weak ferromagnetism and the saturation magnetization ($M_s$) is 52.59 emu/cc, which is similar to the epitaxial $Mn_3Sn$ films.[33] The related research suggests that the weak ferromagnetism of $Mn_3Sn$ films originates from the local tilt of Mn atomic spins within the kagome planes. For further verification of the crystal structure of $Mn_3Sn$, we measured the cross-sectional crystalline structure of the $Mn_3Sn$ layer imaged by high-resolution transmission electron microscopy measurements, as shown in Fig. 1(d). The insets in the bottom right-hand side of Fig. 1(d) show the corresponding fast Fourier transform patterns, which reveal the amorphous phases. Meanwhile, the surface (20 μm×20 μm) morphology of the $Mn_3Sn/Si_3N_4$ film was measured by atomic force microscope, as shown in Fig. 1(e). The results demonstrate that the $Mn_3Sn$ films exhibit relatively flat surface structures, characterized by a root-mean-square roughness of 1.029 nm, which is similar to the previous work.[34]

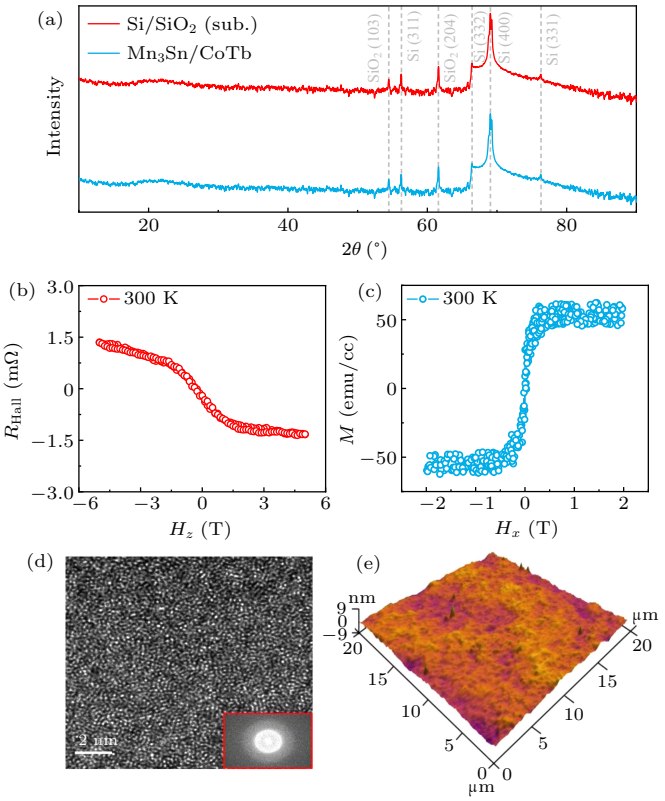



**Fig. 1.** (a) XRD patterns of the sample and silicon substrate. (b) The anomalous Hall resistance ($R_{\rm Hall}$) as a function of the out-of-plane magnetic field ($H_z$) for $Mn_3Sn$ device. (c) Magnetization hysteresis loop of the $Mn_3Sn$ films grown on silicon substrate. (d) High-resolution transmission electron microscopy images of sputtered $Mn_3Sn$ film. The inset shows fast Fourier transform patterns from designated areas. (e) Surface topography of the $Mn_3Sn$ (10 nm) film obtained by atomic force microscopy.

To quantitatively characterize the SOT generated in $Mn_3Sn$, we used standard photolithography and Ar ion beam etching processes to fabricate $Mn_3Sn$/Py into stripe devices with a length of 43.5 μm and a width of 7.7 μm for spin torque ferromagnetic resonance testing. The optical microscope image of the device and a schematic diagram of the spin-torque ferromagnetic resonance testing setup are shown in Fig. 2(a). During the testing, microwave current was injected into the $Mn_3Sn$ sample, generating alternating SOT on the magnetic moments of the Py layer, propelling them into a precessing motion.

The anisotropic magnetoresistance (AMR) effect in the Py layer induces a change in the device resistance corresponding to the current frequency. Under the combined influence of alternating current and resistance, rectified voltage signals $V_{\rm mix}$ can be detected on the device. By scanning the external horizontal magnetic field to induce the ferromagnetic resonance state of the Py layer, the resonance signal curve of $V_{\rm mix}$ with the external magnetic field can be obtained. The value of $V_{\rm mix}$ can be decomposed into a voltage component with a symmetrical line shape and a voltage component with a symmetrical line shape, and is described by the following equation:[35]

$$V_{\rm mix} = V_{\rm s}\frac{\Delta H^2}{\Delta H^2+(H-H_{\rm res})^2} + V_{\rm a}\frac{\Delta H\,(H-H_{\rm res})}{\Delta H^2+(H-H_{\rm res})^2}, \quad (1)$$

where $\Delta H$ and $H_{\rm res}$ represent the linewidth and resonance field. On the right-hand side of Eq. (1), the first term describes a symmetric voltage component with an amplitude $V_{\rm s}$, attributed to in-plane torque. The second term describes an antisymmetric component with an amplitude $V_{\rm a}$, attributed to out-of-plane torque. As show in Fig. 2(b), representative ST-FMR spectra for the simple of $Mn_3Sn$/Py the representative rectification voltage $V_{\rm mix}$ with respect to the external magnetic field are measured at 6 GHz with $\phi_{\rm H} = 30^\circ$ and $210^\circ$, respectively. The obtained result can be well fitted using Eq. (1). Next, to confirm whether there are SOTs generated by spin current components with polarization directions of $y$ ($\sigma_y$), $x$ ($\sigma_x$), and $z$ ($\sigma_z$) in $Mn_3Sn$/Py heterostructures, angle-dependent $V_{\rm mix}$ measurements were systematically conducted for the $Mn_3Sn$/Py bilayer with $\phi_{\rm H}$ ranging from $0^\circ$ to $360^\circ$, as shown in Fig. 2(c).

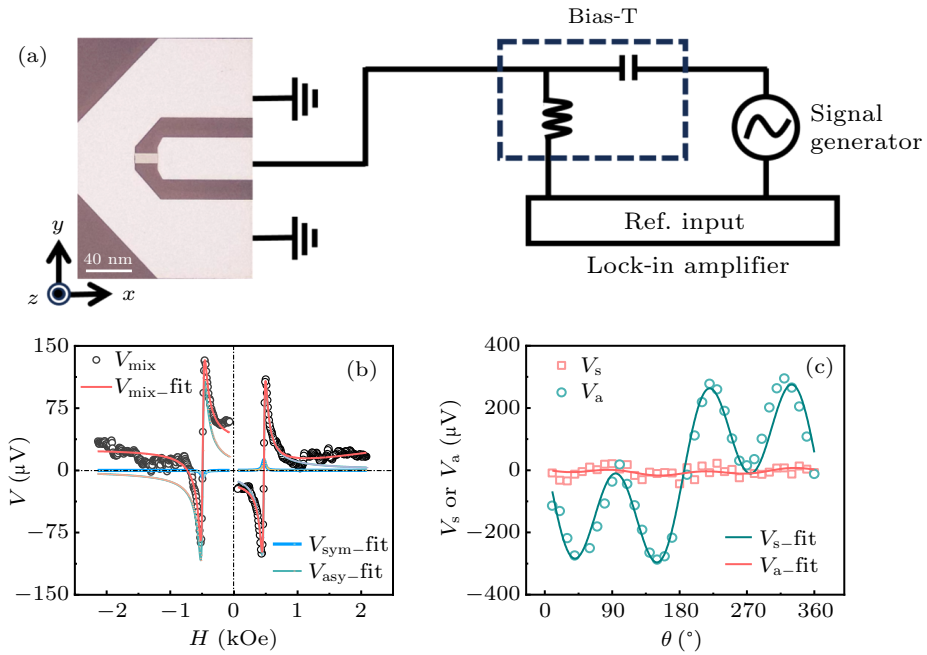



**Fig. 2.** (a) A schematic of the ST-FMR measurement setup. (b) The resonance signal of sample $Mn_3Sn(10)$/Py(7) device at a microwave frequency of 6 GHz and the in-plane magnetic field angle of $30^\circ$ and $210^\circ$ can be decomposed into Lorentz symmetric signal ($V_{\rm s}$) and Lorentz antisymmetric signal ($V_{\rm a}$). (c) $V_{\rm s}$ and $V_{\rm a}$ for the sample as a function of the in-plane magnetic field angle ($\theta$).

Previous studies have demonstrated that the $V_{\rm a}$ and $V_{\rm s}$ voltage signals can be well fitted using the following equation:[8,35,36]

$$\begin{aligned} V_{\rm a} &= A^Y_{\rm FL}\cos\phi_{\rm H}\sin 2\phi_{\rm H} \\ &\quad + A^X_{\rm FL}\sin\phi_{\rm H}\sin 2\phi_{\rm H} + A^Z_{\rm DL}\sin 2\phi_{\rm H}, \quad (2) \\ V_{\rm s} &= S^Y_{\rm DL}\cos\phi_{\rm H}\sin 2\phi_{\rm H} \\ &\quad + S^X_{\rm DL}\sin\phi_{\rm H}\sin 2\phi_{\rm H} + S^Z_{\rm FL}\sin 2\phi_{\rm H}, \quad (3) \end{aligned}$$

where $S^Y_{\rm DL}$, $S^X_{\rm DL}$, and $A^Z_{\rm DL}$ are coefficients for the damping-like torque generated by the $x$ ($\sigma_x$), $y$ ($\sigma_y$), and $z$ ($\sigma_z$) component spin current, respectively. Similarly, $A^Y_{\rm FL}$, $A^X_{\rm FL}$, and $S^Z_{\rm FL}$ correspond to the field-like spin-torque components generated by spin current components with polarization directions of $y$ ($\sigma_y$), $x$ ($\sigma_x$), and $z$ ($\sigma_z$). It should be noted that the coefficient $A^Y_{\rm FL}$ includes the contribution of the field-like torque from both the $y$ ($\sigma_y$) spin current and the Oersted field ($h_{\rm Oe}$). As shown in Fig. 2(c), the test data can be well fitted using Eqs. (2) and (3) to obtain the corresponding coefficients, with the fitting results depicted as solid lines in the same Fig. 2(c), respectively. It should be noted that the variation patterns of $V_{\rm a}$ and $V_{\rm s}$ with $\phi_{\rm H}$ can be described by $\cos\phi_{\rm H}\sin 2\phi_{\rm H}$ function, which confirms that only the SOT generated by the traditional $y$ ($\sigma_y$) direction spin current component exists in the amorphous $Mn_3Sn$ sample. In comparison with epitaxial $Mn_3Sn$ films, the kagome plane orientation is random in amorphous $Mn_3Sn$ films, eliminating the low magnetic structure symmetry. Therefore, no significant SOT is observed from nontraditional $x$ ($\sigma_x$) or $z$ ($\sigma_z$) polarization direction spin current components in amorphous $Mn_3Sn$ samples.

Next, the rectified voltage information at different microwave frequencies was measured at a fixed $\phi_H$ angle of 45°, and the resonance field ($H_{res}$) and linewidth ($\Delta H$) at different microwave frequencies were calculated by Eq. (1), and the results are shown as hollow symbols in Figs. 3(a) and 3(b). Where, resonance field ($H_{res}$) and microwave frequency ($f$) can be described by Kittel equation[35,37]

$$f = \frac{\gamma}{2\pi}\sqrt{H_r(H_r+4\pi M_{eff})}, \tag{4}$$

where $\gamma$ represents the gyromagnetic ratio, and $M_{eff}$ represents the effective saturation magnetization of the ferromagnetic layer. It can be noted that the test data in Fig. 3(a) can be well fitted by Eq. (4), with the effective saturation magnetization of the Py layer obtained by fitting is 3440 Oe. According to the existing experimental results, the linewidth increases linearly with the microwave frequency. The damping constant ($\alpha$) of $Mn_3Sn$/Py heterostructures can be described by the following equation:[38]

$$\Delta H = \Delta H_0 + \frac{4\pi\alpha}{\gamma} f, \tag{5}$$

where $\Delta H$ represents the intrinsic linewidth caused by the inhomogeneity of $Mn_3Sn$. As shown in Fig. 3(b), the black solid line represents the fitted curve and the damping constant ($\alpha$) of $Mn_3Sn$/Py heterostructure is calculated to be 0.0049, which is smaller than that of the amorphous $Pt_xCr_{1-x}$/CoFeB heterostructure. The SOT efficiency of the $Mn_3Sn$/Py heterojunction can be described by the following equation:[35,38]

$$\xi_{SOT} = \frac{S^y_{DL}}{A^y_{FL}} \frac{e\mu_0 M_s t_{Mn_3Sn} t_{FM}}{\hbar} \left[1 + (M_{eff}/H_r)\right]^{\frac{1}{2}}, \tag{6}$$

where $e$ represents the elementary charge, $\hbar$ represents the reduced Planck constant, $t_{Mn_3Sn}$ is the thickness of the $Mn_3Sn$ layer, $t_{FM}$ is the thickness of the Py layer, and $M_s$ represents the saturation magnetization of the Py layer. The SOT efficiency at different microwave frequencies is summarized in Fig. 3(c). The SOT efficiency of the $Mn_3Sn$/Py heterojunction is approximately 0.016 and remains unchanged with varying microwave frequency. This value is similar to that of Pt/Py heterojunction reported previously.

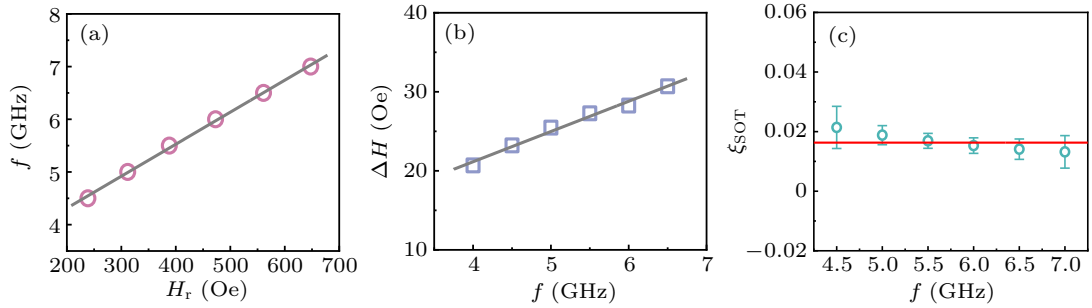



**Fig. 3.** (a) The resonance field ($H_r$) as a function of microwave frequency ($f$). Microwave frequency ($f$) dependence of (b) FMR line width ($\Delta H$) and (c) SOT efficiency ($\xi_{SOT}$). The error bars represent the standard deviations derived from measurements on three devices.

Using SOT to drive perpendicular magnetization switching is a hot topic in spintronics research and also a crucial research content for further development of spin memory devices. Here, we build ferromagnetic CoTb films with perpendicular magnetic anisotropy on amorphous $Mn_3Sn$ films to form $Mn_3Sn$/CoTb heterojunctions. Moreover, to better and more accurately compare the test results, we built a Ta(10)/CoTb(7) control sample. Next, standard lithography and ion beam etching methods were used to fabricate them into Hall bar devices with 8 μm width, as illustrated in the optical microscopy image and test configuration in Fig. 4(a). Then, AHE tests were performed by scanning magnetic fields perpendicular to the film plane ($H_z$), as shown in Fig. 4(b). The test results indicate that the $Mn_3Sn$/CoTb heterojunction exhibits a square anomalous Hall loop, which confirms the good perpendicular magnetic anisotropy of the CoTb layer. As shown in Fig. 4(c), we applied a constant in-plane auxiliary magnetic field ($H_x = 200$ Oe) along the $x$-axis and successfully observed the changes in the high and low configurations of the Hall resistance of the $Mn_3Sn$/CoTb sample by varying the amplitude of the current density injected along the $x$-axis, achieving the SOT driven perpendicular magnetization switching process. Next, we tested the current-driven magnetic moment reversal curves under an auxiliary field ranging from −200 Oe to 200 Oe. It can be noted that within this auxiliary magnetic field range, the current-driven perpendicular magnetization switching process can be achieved. When the auxiliary magnetic field is reversed, the polarity of the current-driven perpendicular magnetization switching also changes, which is a typical characteristic of SOT driven perpendicular magnetization switching. The Ta/CoTb heterojunction also exhibited the same results, indicating that the spin Hall angles of amorphous $Mn_3Sn$ and Ta are opposite. Significantly, we observed that under the same auxiliary magnetic field, the critical switching current density of the $Mn_3Sn$/CoTb heterojunction is lower than that of the Ta/CoTb heterojunction, reaching $3.9\times10^7$ A/cm$^2$. Compared with the Ta/CoTb heterojunction, the decreased critical switching current density observed in $Mn_3Sn$/CoTb could potentially be attributed to its reduced anisotropy field of CoTb.

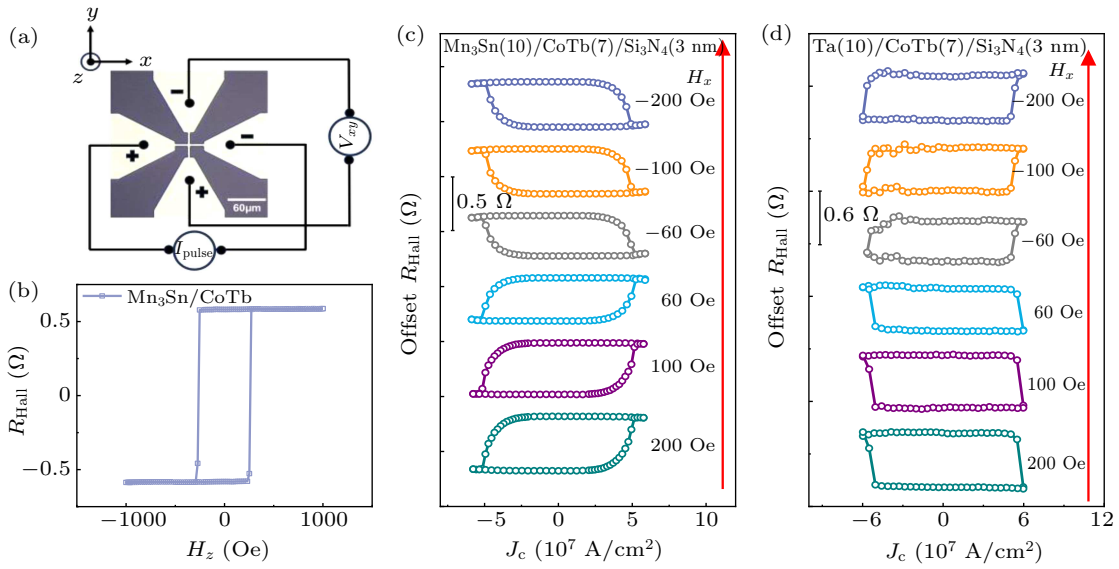



**Fig. 4.** (a) Optical picture of fabricated Hall device and configuration of measurements. (b) The anomalous Hall resistance ($R_{Hall}$) as a function of the out-of-plane magnetic field ($H_z$) for $Mn_3Sn$/CoTb device. SOT-driven perpendicular magnetization switching under different in-plane external fields ($H_x$) for (c) $Mn_3Sn$/CoTb device and (d) Ta/CoTb device.

## 3. Conclusions

In this study, amorphous $Mn_3Sn$ films were deposited onto Si substrates by magnetron sputtering, and the SOT effects in $Mn_3Sn$/Py were quantitatively characterized. The results show that only the $y$ ($\sigma_y$) polarized spin current component of $Mn_3Sn$/Py generates SOT, with a SOT efficiency of 0.016. Next, the current density driven by SOT in amorphous $Mn_3Sn$ can be as low as $3.9\times10^7$ A/cm$^2$, which is smaller than that of Ta/CoTb heterojunctions. This work not only offers a new perspective for investigation SOT in $Mn_3Sn$ films but also advances the practical implementation of $Mn_3Sn$ materials in spin–orbit torque devices.

## Acknowledgements

Project supported by the National Key Research and Development Program of China (Grant No. 2022YFE0103300), the National Natural Science Foundation of China (Grant No. 12274119), the Natural Science Foundation of Hubei Province (Grant No. 2022CFA088), and the Open Research Fund of Songshan Lake Materials Laboratory (Grant No. 2022SLABFN04).

## References

[1] Liu L, Lee O J, Gudmundsen T J, Ralph D C and Buhrman R A 2012 *Phys. Rev. Lett.* **109** 096602
[2] Miron I M, Garello K, Gaudin G, Zermatten P J, Costache M V, Auffret S, Bandiera S, Rodmacq B, Schuhl A and Gambardella P 2011 *Nature* **476** 189
[3] Song C, Zhang R, Liao L Yang, Zhou Y J, Zhou X F, Chen R Y, You Y F, Chen X Z and Pan F 2021 *Prog. Mater. Sci.* **118** 100761
[4] Cao Y, Xing G Z, Lin H, Zhang N, Zheng H Z and Wang K Y 2020 *iScience* **23** 101614
[5] Han X F, Wang X, Wan C H, Yu G Q and Lv X R 2021 *Appl. Phys. Lett.* **118** 120502
[6] Zhou J and Chen J S 2021 *Adv. Electron. Mater.* **7** 2100465
[7] Bangar H, Khan K I A, Kumar A, Chowdhury N, Muduli P K and Muduli P K 2022 *Adv. Quantum Technol.* **6** 2200115
[8] Hu S, Shao D F, Yang H L, Pan C, Fu Z X, Tang M, Yang Y M, Fan W J, Zhou S M, Tsymbal E Y and Qiu X P 2022 *Nat. Commun.* **13** 4447
[9] Kondou K, Chen H, Tomita T, Ikhlas M, Higo T, Macdonald A H, Nakatsuji S and Otani Y C 2021 *Nat. Commun.* **12** 6491
[10] Deng Y C, Liu X H, Chen Y Y, Du Z Z, Jiang N, Shen C, Zhang E Z, Zheng H Z, Lu H Z and Wang K Y 2023 *Natl. Sci. Rev.* **10** nwac154
[11] Cao C M, Chen S W, Xiao R C, Zhu Z T, Yu G Q, Wang Y P, Qiu X P, Liu L, Zhao T Y, Shao D F, Xu Y, Chen J S and Zhan Q F 2023 *Nat. Commun.* **14** 5873
[12] Wang X N, Yan H, Zhou X R, Chen H Y, Feng Z X, Qin P X, Meng Z A, Liu L and Liu Z Q 2022 *Mater. Today Phys.* **28** 100878
[13] Nakatsuji S, Kiyohara N and Higo T 2015 *Nature* **527** 212
[14] Xu T, Bai H, Dong Y Q, Zhao L, Zhou H A, Zhang J W, Zhang X X and Jang W J 2023 *APL Mater.* **11** 071116
[15] Zhang W F, Han W, Yang S H, Sun Y, Zhang Y, Yan B H and Parkin S S P 2016 *Sci. Adv.* **2** e1600759
[16] Kimata M, Chen H, Kondou K, Sugimoto S, Muduli P K, Ikhlas M, Omori Y, Tomita T, Macdonald A H, Nakatsuji S and Otani Y 2019 *Nature* **565** 627
[17] Hajiri T, Matsuura K, Sonoda K, Tanaka E, Ueda K and Asano H 2021 *Phys. Rev. Appl.* **16** 024003
[18] Liu Z Q, Chen H, Wang J M, Liu J H, Wang K, Feng Z X, Yan H, Wang X R, Jiang C B, Coey J M D and Macdonald A H 2018 *Nat. Electron* **1** 172
[19] Ikhlas M, Tomita T, Koretsune T, Suzuki M T, Nishio-Hamane D, Arita R, Otani Y and Nakatsuji S 2017 *Nat. Phys.* **13** 1085
[20] Miyasato T, Abe N, Fujii T, Asamitsu A, Onoda S, Onose Y, Nagaosa N and Tokura Y 2007 *Phys. Rev. Lett.* **99** 086602
[21] Pu Y, Chiba D, Matsukura F, Ohno H and Shi J 2008 *Phys. Rev. Lett.* **101** 117208
[22] Sakuraba Y, Hasegawa K, Mizuguchi M, Kubota T, Mizukami S, Miyazaki T and Takanashi K 2013 *Appl. Phys. Express* **6** 033003
[23] Hasegawa K, Mizuguchi M, Sakuraba Y, Kamada T, Kojima T, Kubota T, Mizukami S, Miyazaki T and Takanashi K 2015 *Appl. Phys. Lett.* **106** 252405
[24] Qin P X, Yan H, Wang X N, Chen H Y, Meng Z A, Dong J T, Zhu M, Cai J L, Feng Z X, Zhou X R, Liu L, Zhang T L, Zeng Z M, Zhang J, Jiang C B and Liu Z Q 2023 *Nature* **613** 485
[25] Zhao H C Xia H, Hu S, Lv Y Y, Zhao Z R, He J, Liang E, Ni G, Chen L Y, Qiu X P, Zhou S M and Zhao H B 2021 *Nat. Commun.* **12** 5266
[26] Kuroda K, Tomita T, Suzuki M T, *et al.* 2017 *Nat. Mater.* **16** 1090
[27] Wang X H, Hossain M T, Thapaliya T R, Khadka D, Lendinez S, Chen H, Doty M F, Jungfleisch M B, Huang S X, Fan X and Xiao J Q 2023 *Phys. Rev. Mater.* **7** 034404

[28] Hibino Y, Taniguchi T, Yakushiji K, Fukushima A, Kubota H and Yuasa S 2020 *Phys. Rev. Appl.* **14** 064056

[29] Binda F, Fedel S, Alvarado S F, Noel P and Gambardella P 2023 *Adv. Mater.* **35** 2304905

[30] Hu C Y, Chiu Y F, Tsai Chia C, Huang C C, Chen K H, Peng C W, Lee C M, Song M Y, Huang Y L, Lin S J and Pai C F 2022 *ACS Appl. Electron. Mater.* **4** 1099

[31] Peng C W, Liao W B, Chen T Y and Pai C F 2021 *ACS Appl. Mater. Interfaces* **13** 15950

[32] Feng Z X, Zhou X R, Šmejkal L, Wu L, Zhu Z W, Guo H X, González-Hernández R, Wang X N, Yan H, Qin P X, Zhang X, Wu H J, Chen H Y, Meng Z A, Liu L, Xia Z C, Sinova J, Jungwirth T and Liu Z Q 2022 *Nat. Electron.* **5** 735

[33] You Y F, Chen X Z, Zhou X F, Gu Y D, Zhang R Q, Pan F and Song C 2019 *Adv. Electron. Mater.* **5** 1800818

[34] Higo T, Qu D R, Li Y F, Chien C L, Otani Y and Satoru N 2018 *Appl. Phys. Lett.* **113** 202402

[35] Liu L Q, Moriyama T, Ralph D C and Buhrman R A 2011 *Phys. Rev. Lett.* **106** 036601

[36] Zhou J, Shu X Y, Liu Y H, Wang X, Lin W N, Chen S H, Liu L, Xie Q D, Hong T, Yang P, Yan B H, Han X F and Chen J S 2020 *Phys. Rev. B* **101** 184403

[37] Sklenar J, Zhang W, Jungfleisch M B, Jiang W J, Chang H C, Pearson J E, Wu M Z, Ketterson J B and Hoffmann A 2015 *Phys. Rev. B* **92** 174406

[38] Wang Y, Ramaswamy R and H Yang 2018 *J. Phys. D: Appl. Phys.* **51** 273002